

## Measurement of Mechanical Deformations Induced by Enhanced Electromagnetic Stress on a Parallel Metallic-Plate System

M. Wang,<sup>1,2</sup> S. Wang,<sup>1,3</sup> Q. Zhang,<sup>1,2</sup> C. T. Chan,<sup>1</sup> and H. B. Chan<sup>1,2,\*</sup>

<sup>1</sup>*Department of Physics, The Hong Kong University of Science and Technology, Clear Water Bay, Kowloon, Hong Kong, China*

<sup>2</sup>*William Mong Institute of Nano Science and Technology, The Hong Kong University of Science and Technology, Clear Water Bay, Kowloon, Hong Kong, China*

<sup>3</sup>*Department of Physics, City University of Hong Kong, Tat Chee Avenue, Kowloon, Hong Kong, China*



(Received 28 March 2018; published 17 July 2018)

We measured the electromagnetic stress-induced local strain distribution on a centimeter-sized parallel-plate metallic resonant unit illuminated with microwave radiation. Using a fiber interferometer, we found that the strain changes sign across the resonant unit, in agreement with theoretical predictions that the attractive electric and repulsive magnetic forces act at different locations. The enhancement of the corresponding maximum local electromagnetic stress is stronger than the enhancement of the net force, reaching a factor of  $> 600$  compared to the ordinary radiation pressure.

DOI: [10.1103/PhysRevLett.121.035502](https://doi.org/10.1103/PhysRevLett.121.035502)

Recent advances in metamaterials have opened up a new paradigm for manipulating light or sound using functionalities not achievable with conventional materials. Familiar examples include negative refraction [1,2] and cloaking [2,3]. Active tunability of electromagnetic (EM) properties of metamaterials holds promise in taking the wave manipulation functionality to the next level. Such active control can be realized by manipulating the shape or the relative positions of the building blocks [4,5]. Various actuation mechanisms that utilize thermal [6,7], electrostatic [8–10], magnetic [11], or mechanical [12] effects have been proposed or demonstrated. Alternatively, one can also exploit the mechanical effects induced by the EM radiation [13–24]. At resonance, the EM field can be strongly concentrated at certain locations of the metamaterial elements. The associated mechanical effects could be significantly enhanced. Such large enhancement is of importance to the field of optomechanics [25] and opens new opportunities for nonlinear [18,26] or reconfigurable [6–9,11] metamaterials, where EM force are used to control photonic structures.

While it is well established that the net EM force acting on a resonating element by a time-harmonic external field can be much larger than the ordinary radiation force [13,15,16,22,24,27,28], there are recent predictions that enhancements in the local EM stress can be even stronger [29]. Such notions are based on the fact that the electric and magnetic forces, which are generated by the oscillating charges and currents, respectively, tend to have opposite directions at resonance. Since these two forces act on different parts of the resonating element, the local stress is expected to significantly exceed the average pressure which is in fact a remnant of the imperfect cancellation of the electric and magnetic forces [15].

Apart from the practical goal of generating a large mechanical response, measurement of the local EM stress exerted on metamaterials is also of fundamental interest. It is well known that the time-averaged net EM force on an isolated object can be calculated by integrating the EM stress tensor across any boundary in vacuum that completely encloses the object. Using any EM stress tensor (e.g., the Maxwell tensor, the Helmholtz tensor, or the Minkowski tensor) gives the same net EM force. However, there is no general recipe for calculating the local stress. For general dielectric materials, it is not yet clear which stress tensor should be used. In fact, it has been predicted that for electrostrictive materials, the Maxwell stress tensor is not applicable [30,31]. Such ambiguity is also related to complicated issues involving kinetic and canonical EM momentum inside a dielectric media and subtle differences between microscopic and macroscopic fields. Measurement of the EM stress, on the other hand, is often complicated by thermal effects that can dominate the mechanical response [22,24]. Separating the EM and thermal contributions has proven to be nontrivial. To our knowledge, the local EM stress exerted on a resonating unit of a metamaterial has not yet been measured.

In this Letter, we report measurement of the deformation of a system consisting of centimeter-sized gold parallel plates induced by the time-averaged EM stress of incident microwave radiation. The local deformation is measured by scanning a fiber interferometer across the top plate. We distinguish contributions of the EM stress induced by the microwave radiation from thermal effects that generate an additional phase lag in the mechanical vibrations [32]. The measured EM strain distribution is found to change sign across the plate, in agreement with theoretical predictions [29] that the attractive electric force and the repulsive

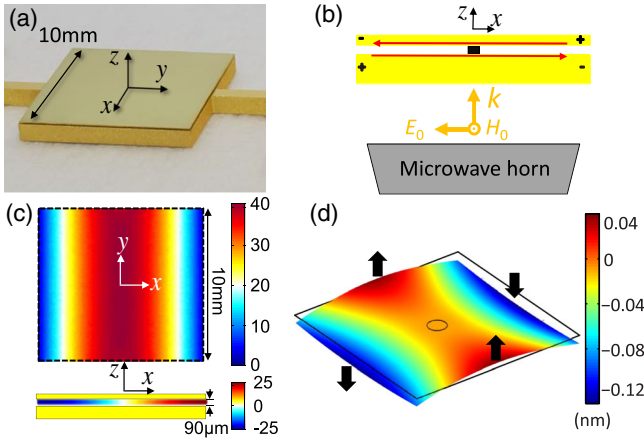


FIG. 1. (a) The double-plate resonating unit. The thick bottom plate is connected to the support by two rods. (b) Cross-sectional view of the double plate system (not to scale), showing induced antiparallel currents (red arrows) and charges at resonance. A silicon post supports the top plate at the middle. (c) The magnetic field (along the  $y$  direction) distribution in the gap at resonance (top) and the corresponding electric field (along the  $z$  direction) distribution along the middle of the plate (bottom). Both are normalized to the incident field amplitude. (d) Calculated deformation of the top plate in response to the time-averaged electromagnetic stress. The black arrows represent the directions of the stress at the middle of the four edges.

magnetic force are concentrated at different locations. At the microwave resonance frequency, the net EM force on the plate is enhanced by a factor of  $\sim 20$  relative to the conventional radiation force while the enhancement of EM stress reaches a factor of  $> 600$ .

Figure 1(a) shows the parallel-plate resonant unit in our experiment. It consists of a thin plate of thickness  $68 \mu\text{m}$  made entirely of gold and a copper bottom plate that is much thicker (1 mm) and uniformly coated with  $1.2 \mu\text{m}$  gold. Both plates measure 10 mm by 10 mm in the  $x$ - $y$  plane. As assembled, the gap between the two plates is  $\sim 90 \mu\text{m}$ , defined by a cylindrical silicon column of radius  $500 \mu\text{m}$  that is glued to the two plates. The two plates serve as the resonant cavity that confines the EM field. Only the thin top plate shows detectable deformation. Two rods are connected to the left and right edges of the thick bottom plate [Fig. 1(a)], providing mechanical support.

As shown in the bottom part of Fig. 1(b), a microwave horn is placed 5 mm below the bottom plate. It emits microwave radiation with electric field, magnetic field, and wave vector along the  $x$ ,  $y$ , and  $z$  directions, respectively. At resonance, the EM energy stored between the two plates attains a maximum. Figure 1(c) shows the calculated magnetic field and electric field in the gap for the anti-symmetric mode of the cavity where antiparallel oscillating currents are generated on the two plates due to the time-varying magnetic flux in the  $y$  direction. Because of the current flow, opposite charges accumulate periodically on the edges of the plates, as shown in Fig. 1(b). The

antiparallel currents generate a repulsive magnetic force near the middle of the plates while the opposite accumulated charges lead to an attractive electric force near the edges. Previous works focused on the enhancement of the net force that results from the incomplete cancellation of the time-averaged attractive electric and repulsive magnetic forces [22]. Our goal here is to measure the local stress and to demonstrate that local forces can achieve even stronger enhancement by exploiting the different spatial distribution of the electric and magnetic forces. Calculations (Supplemental Material [33]) indicate that the maximum stress is enhanced by a factor of more than 600 times over the ordinary photon pressure, compared to the enhancement factor of about 20 for the net EM force. Figure 1(d) shows the calculated deformation of the plate in response to the stress exerted by the EM field. With the center of the plate fixed by the supporting post, the left and right edges bend downwards due to the electric force while the top and bottom edges bend upwards due to the magnetic force.

A fiber interferometer working at a wavelength of 1550 nm is used to measure the deformation at different locations across the plate (Supplemental Material [33]). As shown in Fig. 2(a), the device and the microwave horn are scanned along the  $X$ - $Y$  direction by positioners. By maximizing the mechanical response, the microwave resonance frequency of the parallel-plate system is determined to be 14.57 GHz. The intensity of the microwave radiation is modulated at  $\omega$ , generating a periodic stress on the top plate. Vibrations of the top plate leads to periodic modulations of the reflected light intensity in the fiber interferometer. The light intensity is measured with a photodetector, the output of which is connected to a lockin amplifier referenced at  $\omega$ . Measurements are performed at room temperature and pressure of  $< 10^{-5}$  torr giving negligible viscous damping.

The equation of motion for the top plate is [34]

$$D\nabla^4 A + \rho h \frac{\partial^2 A}{\partial t^2} + \gamma \frac{\partial A}{\partial t} = P(\vec{r}, t), \quad (1)$$

where  $A(\vec{r}, t)$  is the local displacement perpendicular to the substrate,  $\rho$  is the mass density, and  $h$  is the thickness of the plate. Here,  $D = Y_g h^3 / [12(1 - \nu^2)]$  is the flexural rigidity, with  $Y_g$  being the Young's modulus and  $\nu$  being the Poisson ratio. The damping term is proportional to the local velocity with proportionality constant  $\gamma$ . For periodic excitation  $P(\vec{r}, t) = P_0(\vec{r}) \cos(\omega t)$  at a modulation frequency  $\omega$ ,  $A(\vec{r}, t)$  can be written as

$$A(\vec{r}, t) = U(\vec{r}) \cos(\omega t) - V(\vec{r}) \sin(\omega t), \quad (2)$$

where  $U(\vec{r})$  and  $V(\vec{r})$  are the spatial distribution of the amplitude of vibrations in-phase and out-of-phase with  $P$ . By solving Eq. (1), we get the response of the plate as a

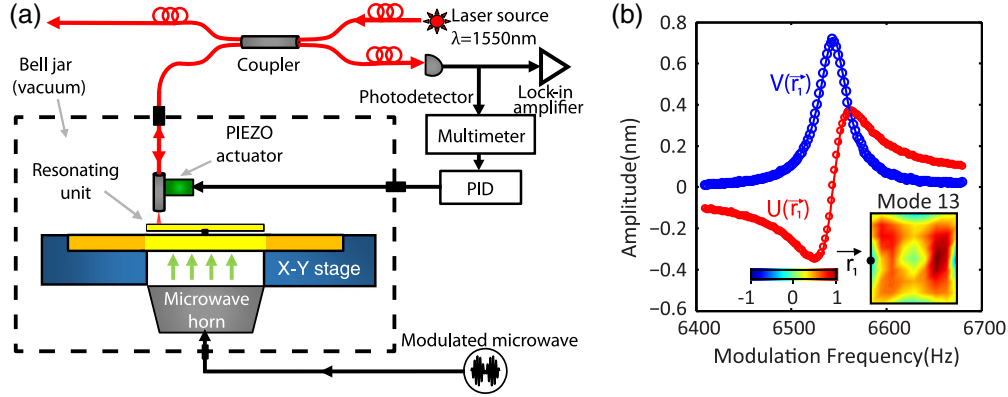


FIG. 2. (a) Local deformation of the top plate is measured by a fiber interferometer. The location of measurement is controlled by an X-Y positioning stage. (b) Vibration amplitude of the top plate in-phase ( $U$ , red) and out-of-phase ( $V$ , blue) with the intensity modulations of the microwave radiation at location  $\vec{r}_1$  for normal mode 13. Inset: the measured mode shape for mode 13, normalized to the maximum vibration amplitude across the plate.

linear combination of all the normal modes (Supplemental Material [33]):

$$U(\vec{r}, \omega) + iV(\vec{r}, \omega) = \sum_n \frac{A_n(\vec{r})}{1 - (\omega/\omega_n)^2 + i[\omega/(\omega_n Q_n)]}, \quad (3)$$

where  $\omega_n$  and  $Q_n = \rho h \omega_n / \gamma$  are the resonance frequency and the effective quality factor of the  $n$ th mode, respectively. As we discuss later,  $A_n(\vec{r})$  represents the contribution of the  $n$ th mode. In our system,  $Q_n$ 's are rather large ( $> 120$ ), so that when  $\omega$  is close to  $\omega_n$ , the response of the plate is dominated by mode  $n$ . Figure 2(b) plots  $U(\vec{r}_1)$  and  $V(\vec{r}_1)$  measured at one particular location  $\vec{r}_1$  (marked in the inset) for mode 13. Since the displacement of mode 13 is negative (towards the thick plate) at  $\vec{r}_1$ , both  $U(\vec{r}_1)$  and  $V(\vec{r}_1)$  pick up an extra negative sign when compared to the response of a driven harmonic oscillator.

The insets of Fig. 3(a) shows the normalized spatial distribution  $s_n(\vec{r})$  of a few modes ( $n = 4, 5, 7$ ) calculated with finite element analysis (Supplemental Material [33]). They are in good agreement with the measured  $s_n(\vec{r})$  that is excited by the incident microwave with intensity modulated at  $\omega_n$  [insets in Fig. 3(b)]. Unless otherwise stated, the microwave frequency is fixed at the resonant value of 14.57 GHz. The microwave power is 250 mW.

The main plot in Fig. 3(a) shows the  $\omega$  dependence of the calculated vibration amplitude  $R = \sqrt{U^2(\vec{r}_1, \omega) + V^2(\vec{r}_1, \omega)}$  at location  $\vec{r}_1$ . For each mode, the contribution to the overall vibrational response  $A_n(\vec{r})$  is determined by the overlap of the mode profile  $s_n(\vec{r})$  with  $P_0(\vec{r})$ :

$$A_n(\vec{r}) = \frac{1}{\rho h \omega_n^2} s_n(\vec{r}) \iint s_n^*(\vec{r}') P_0(\vec{r}') dx' dy'. \quad (4)$$

In other words, the relative heights of the peaks in Fig. 3(a) depend on the spatial distribution of the applied stress  $P_0(\vec{r})$ . Since the stress exerted by the microwave radiation is symmetric about both the X and Y axes, only vibration modes with the same symmetry can be excited. Figure 3(b) shows the measurements, with these symmetric modes plotted in red. The antisymmetric modes (antisymmetric about the X and/or Y axis) are plotted in blue. They are dark modes in the numerical simulations, as shown by their absence in Fig. 3(a). In experiments, our device is not perfectly symmetric as neither the gold plate thickness nor the gap is exactly uniform. Therefore, the antisymmetric modes can also be excited.

One approach to obtain the strain induced by the EM wave is to measure the response at dc (i.e., zero modulation frequency). However, we find that as  $\omega$  is reduced towards zero photothermal effects become dominant, as evident by the rise at low frequencies depicted in black in Fig. 3(b). At the microwave resonance, the radiation exerts strong EM stress  $P_{EM}$  that originates from the enhanced current and charge oscillations. This current also leads to Ohmic heating and thermal expansion. The thermal deformations induced by radiation are commonly associated with photothermal forces. Unlike the EM force that appears instantaneously once the radiation is turned on, the mechanical deformation induced by the photothermal force exhibits a delay. Assuming a delayed impulse response of  $h(t) = 1 - \exp(-t/\tau)$ , the photothermal stress can be written as [32]

$$P_{\text{thermal}}(\vec{r}, t) = \int_0^t c(\vec{r}, t') \frac{dI(t')}{dt'} h(t - t') dt', \quad (5)$$

where  $I$  is the intensity of the microwave and  $c$  characterizes the spatial distribution of the photothermal stress. With the contribution of the photothermal stress included, Eq. (3) is modified to

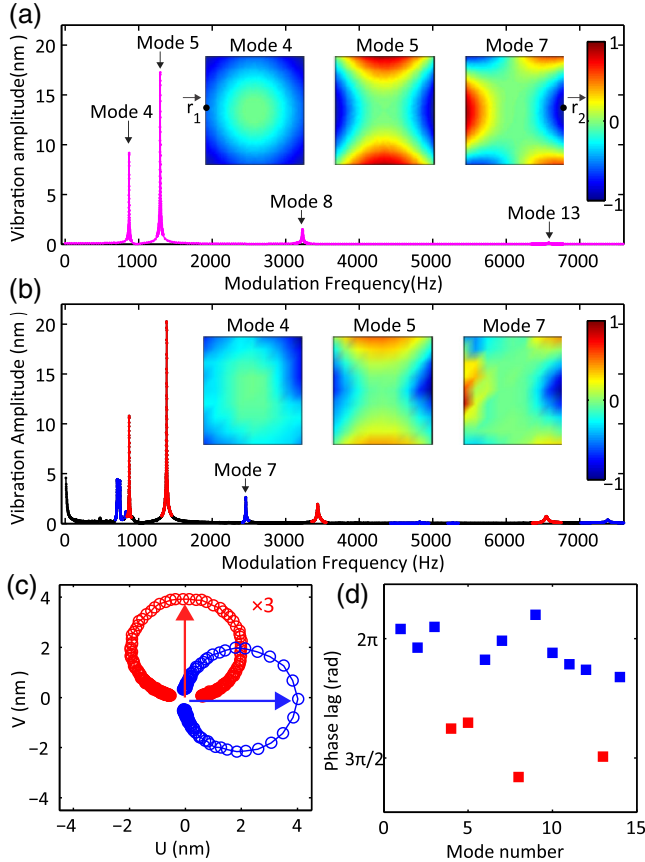


FIG. 3. (a) Calculated vibration amplitude at location  $\vec{r}_1$  in response to the electromagnetic stress as a function of microwave modulation frequency. Insets: the normalized mode profiles for normal modes 4, 5, and 7 for the 8 mm by 8 mm area at the center of the plate. (b) Measured vibration amplitude. The red (blue) peak represents a mode with the same (opposite) symmetry as the electromagnetic stress. Insets: measured mode profiles for modes 4, 5, and 7. (c) Response of modes 13 (red) and 7 (blue) at location  $\vec{r}_2$  plotted in the  $U$ - $V$  phase space. The red (blue) arrow indicates the vibrations lag the microwave modulation by  $3\pi/2$  ( $2\pi$ ). (d) Measured phase lags of the first 14 normal modes, plotted in red (blue) for modes with the same (different) symmetry as the EM stress. Error bars are comparable to the symbol size.

$$U(\vec{r}, \omega) + iV(\vec{r}, \omega) = \sum_n \frac{A_{EM,n}(\vec{r}) + \frac{A_{\text{thermal},n}(\vec{r})}{(1+i\omega\tau)}}{1 - (\omega/\omega_n)^2 + i[\omega/(\omega_n Q_n)]}, \quad (6)$$

where  $A_{EM,n}$  and  $A_{\text{thermal},n}$  characterize the vibration amplitude of the  $n$ th mode excited by the EM stress and photothermal stress, respectively. The sharp increase of the vibration amplitude as  $\omega$  is lowered towards zero indicates that  $A_{\text{thermal},n}(\vec{r}) \gg A_{EM,n}(\vec{r})$  at dc. By fitting to the low frequency region in Fig. 3(b), we find that  $\tau = 132$  ms. Measurements at other locations yield similar values.

Our device is designed to have mode eigenfrequencies much higher than  $1/\tau$  (e.g.,  $\omega_1/2\pi = 708$  Hz), so that  $\omega_n\tau \gg 1$  for all modes. At modulation frequency  $\omega \sim \omega_n$ , the photothermal term in the numerator of Eq. (6) is reduced to  $-iA_{\text{thermal},n}(\vec{r})/(\omega\tau)$ . Apart from decreasing rapidly with  $\omega$ , the photothermal contribution to the vibrations lags behind that induced directly by the EM stress by an extra phase of  $\pi/2$ . Figure 3(c) compares the phase of vibrations of modes 13 and 7 at location  $\vec{r}_2$  where the displacement is negative (towards the thick plate). For mode 13, the phase of  $3\pi/2$  is consistent with the notion that vibrations are excited largely by the EM stress because this mode possesses the same symmetry [inset of Fig. 2(b)] as the EM stress. In contrary, mode 7 has odd symmetry about the  $y$  axis [right inset in Fig. 3(a)]. Interestingly, the phase of vibrations lags behind mode 13 by  $\pi/2$ . Figure 3(d) shows that, in general, the phase lag at the eigenfrequencies of the antisymmetric modes (blue squares) relative to the modulation is close to  $2\pi$ , larger than that of the symmetric modes by  $\sim\pi/2$  (red squares). The symmetric and antisymmetric modes are therefore predominately excited by the EM stress and the photothermal effect, respectively (Supplemental Material [33]).

The extra  $\pi/2$  phase lag of the photothermal response in our system for  $\omega > 1/\tau$  allows us to exclude the photothermal contribution to the deformation for each mode and extrapolate the remaining part back to zero frequency to obtain the strain induced solely by the EM stress. Specifically, we set the modulation frequency to  $\omega_n$  so that the complex amplitude of vibrations described by the series summation in Eq. (6) are dominated by a single mode  $n$ :

$$\begin{aligned} U(\vec{r}, \omega_n) &= -Q_n A_{\text{thermal},n}(\vec{r})/(\omega_n\tau) \\ V(\vec{r}, \omega_n) &= -Q_n A_{EM,n}(\vec{r}). \end{aligned} \quad (7)$$

Equation (7) shows that  $A_{EM,n}(\vec{r})$  can be obtained by dividing the measured vibration amplitude  $V(\vec{r}, \omega_n)$  out-of-phase with the microwave modulation at  $\omega_n$  by the quality factor  $Q_n$ . By measuring  $A_{EM,n}(\vec{r})$  for all the modes and setting both  $\omega$  and  $A_{\text{thermal},n}(\vec{r})$  in Eq. (6) equal to zero, the deformation  $A_{EM}(\vec{r})$  induced solely by the EM stress can be obtained:

$$A_{EM}(\vec{r}) = \sum_n A_{EM,n}(\vec{r}). \quad (8)$$

Figure 4(a) shows  $A_{EM}(\vec{r})$  measured using the above procedure, with the summation up to  $n = 14$ . The largest contribution comes from the symmetric modes, especially modes 4 and 5 (Supplemental Material [33]). The strain distribution agrees well with calculations [Fig. 4(b)] (Supplemental Material [33]). In particular, the sign of the deformation changes for different locations on the plate. The induced currents concentrated near the middle of the upper and lower edges lead to repulsive magnetic forces, while charges on the left and right edges generate attractive electric forces.

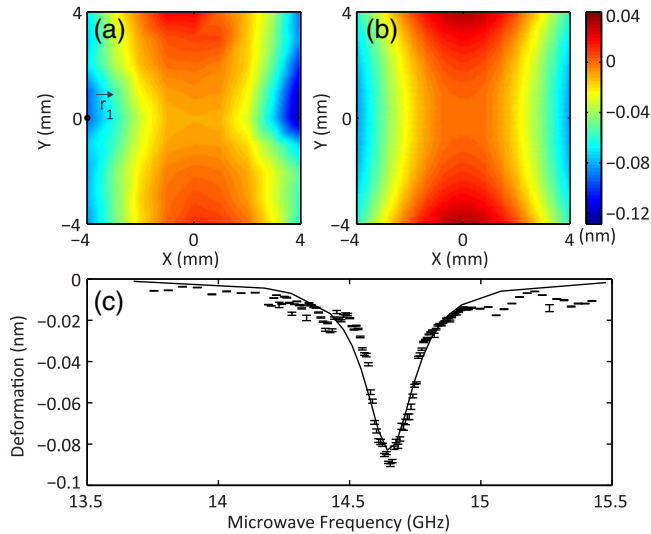


FIG. 4. (a) Measured and (b) calculated strain of the top plate induced by the electromagnetic stress. (c) Dependence of the deformation of the top plate at location  $\vec{r}_1$  on the microwave frequency. The solid line shows the calculated results.

The time-averaged stress exerted by the EM radiation, in principle, can be deduced by inserting the measured  $A_{EM}(\vec{r})$  to the equation of motion of the plate [Eq. (1)] and setting the partial time derivatives to zero. However, this procedure involves taking fourth order derivatives, and the calculated stress from our data is too noisy for any meaningful discussion. Instead, we draw a number of conclusions on the EM force or stress based on the good agreement between the measured and predicted strain. First, the imperfect cancellation of the attractive and repulsive stress produces a net EM force of 24.8 nN (for 250 mW incident microwave power), about 20 times larger than ordinary photon force. Second, our experiment demonstrates that the deformation of the plate is consistent with local EM stress that shows even larger enhancement. The maximum stress, exerted at location  $\vec{r}_1$  in Fig. 4(a), is more than 600 times larger than ordinary photon pressure. These enhancements only take place at the microwave resonance when the EM waves are concentrated between the two plates. As shown in Fig. 4(c), as the microwave frequency is tuned away from resonance, the deformation of the plate drastically decreases, in agreement with calculations.

In summary, our experiment demonstrated that the local strain induced by the electromagnetic field on a parallel-plate resonating system is of different sign across the plate. At certain locations, the corresponding EM induced stress is significantly stronger than the already-enhanced average pressure. Our work provides a general recipe for isolating the EM stress from the photothermal stress. In our system, the stress is well described by the Maxwell stress tensor because the EM field inside the material is essentially zero [29]. The ability to measure EM stress-induced local deformations opens possibilities to test theoretical

predictions of EM stress in configurations where the Maxwell stress tensor is not applicable [30,31].

Strongly enhanced EM stress could provide a new mechanism to achieve tunable or nonlinear metamaterials [18,26], where large shifts in the EM resonance can be induced by mechanical deformations. An important advantage of EM stress over photothermal stress is that for the former the speed of mechanical response is not limited by the thermal time constants of the system.

This work is supported by Grant No. AoE/P-02/12 from the Research Grants Council of Hong Kong SAR. S. W. is also supported by a grant from City University of Hong Kong (Project No. 9610388).

\*hochan@ust.hk

- [1] J. B. Pendry, *Contemp. Phys.* **45**, 191 (2004).
- [2] R. A. Shelby, D. R. Smith, and S. Schultz, *Science* **292**, 77 (2001).
- [3] H. Chen, C. T. Chan, and P. Sheng, *Nat. Mater.* **9**, 387 (2010).
- [4] N. I. Zheludev and Y. S. Kivshar, *Nat. Mater.* **11**, 917 (2012).
- [5] N. I. Zheludev and E. Plum, *Nat. Nanotechnol.* **11**, 16 (2016).
- [6] H. Tao, A. C. Strikwerda, K. Fan, W. J. Padilla, X. Zhang, and R. D. Averitt, *Phys. Rev. Lett.* **103**, 147401 (2009).
- [7] J.-Y. Ou, E. Plum, L. Jiang, and N. I. Zheludev, *Nano Lett.* **11**, 2142 (2011).
- [8] J.-Y. Ou, E. Plum, J. Zhang, and N. I. Zheludev, *Nat. Nanotechnol.* **8**, 252 (2013).
- [9] Y. H. Fu, A. Q. Liu, W. M. Zhu, X. M. Zhang, D. P. Tsai, J. B. Zhang, T. Mei, J. F. Tao, H. C. Guo, X. H. Zhang, J. H. Teng, N. I. Zheludev, G. Q. Lo, and D. L. Kwong, *Adv. Funct. Mater.* **21**, 3589 (2011).
- [10] W. Zhu, A. Liu, T. Bourouina, D. Tsai, J. Teng, X. Zhang, G. Lo, D. Kwong, and N. Zheludev, *Nat. Commun.* **3**, 1274 (2012).
- [11] J. Valente, J.-Y. Ou, E. Plum, I. J. Youngs, and N. I. Zheludev, *Appl. Phys. Lett.* **106**, 111905 (2015).
- [12] J. Li, C. M. Shah, W. Withayachumnankul, B. S. -Y. Ung, A. Mitchell, S. Sriram, M. Bhaskaran, S. Chang, and D. Abbott, *Appl. Phys. Lett.* **102**, 121101 (2013).
- [13] R. Zhao, P. Tassin, T. Koschny, and C. M. Soukoulis, *Opt. Express* **18**, 25665 (2010).
- [14] G. Volpe, R. Quidant, G. Badenes, and D. Petrov, *Phys. Rev. Lett.* **96**, 238101 (2006).
- [15] S. B. Wang, J. Ng, H. Liu, H. H. Zheng, Z. H. Hang, and C. T. Chan, *Phys. Rev. B* **84**, 075114 (2011).
- [16] H. Liu, J. Ng, S. B. Wang, Z. F. Lin, Z. H. Hang, C. T. Chan, and S. N. Zhu, *Phys. Rev. Lett.* **106**, 087401 (2011).
- [17] J. Kohoutek, D. Dey, A. Bonakdar, R. Gelfand, A. Sklar, O. G. Memis, and H. Mohseni, *Nano Lett.* **11**, 3378 (2011).
- [18] M. Lapine, I. V. Shadrivov, D. A. Powell, and Y. S. Kivshar, *Nat. Mater.* **11**, 30 (2012).
- [19] Y. He, S. He, J. Gao, and X. Yang, *Opt. Express* **20**, 22372 (2012).

- [20] J. Zhang, K. F. MacDonald, and N. I. Zheludev, *Phys. Rev. B* **85**, 205123 (2012).
- [21] V. Gini, P. Tassin, C. M. Soukoulis, and I. Veretennicoff, *Phys. Rev. Lett.* **110**, 057401 (2013).
- [22] Z. Marcet, Z. H. Hang, S. B. Wang, J. Ng, C. T. Chan, and H. B. Chan, *Phys. Rev. Lett.* **112**, 045504 (2014).
- [23] D. Ma, J. L. Garrett, and J. N. Munday, *Appl. Phys. Lett.* **106**, 091107 (2015).
- [24] D. Guan, Z. H. Hang, Z. Marcet, H. Liu, I. I. Kravchenko, C. T. Chan, H. B. Chan, and P. Tong, *Sci. Rep.* **5**, 16216 (2015).
- [25] M. Aspelmeyer, T. J. Kippenberg, and F. Marquardt, *Rev. Mod. Phys.* **86**, 1391 (2014).
- [26] J.-Y. Ou, E. Plum, J. Zhang, and N. I. Zheludev, *Adv. Mater.* **28**, 729 (2016).
- [27] R.-c. Jin, J. Li, Y.-h. Wang, M.-j. Zhu, J.-q. Li, and Z.-g. Dong, *Opt. Express* **24**, 27563 (2016).
- [28] J. Zhang, K. F. MacDonald, and N. I. Zheludev, *Opt. Lett.* **39**, 4883 (2014).
- [29] S. B. Wang and C. T. Chan, *J. Phys. D* **46**, 395104 (2013).
- [30] W. Sun, S. B. Wang, J. Ng, L. Zhou, and C. T. Chan, *Phys. Rev. B* **91**, 235439 (2015).
- [31] S. Wang, J. Ng, M. Xiao, and C. T. Chan, *Sci. Adv.* **2**, e1501485 (2016).
- [32] C. H. Metzger and K. Karrai, *Nature (London)* **432**, 1002 (2004).
- [33] See Supplemental Material at <http://link.aps.org/supplemental/10.1103/PhysRevLett.121.035502>, for details on the derivation of the mechanical response of the plate, the measurement of local strain by fiber interferometer, the calculation of EM stress and induced strain, and the contributions of the symmetric/anti-symmetric modes to the induced strain.
- [34] A. W. Leissa, *Vibration of Plates*, NASA SP-160 (1969).